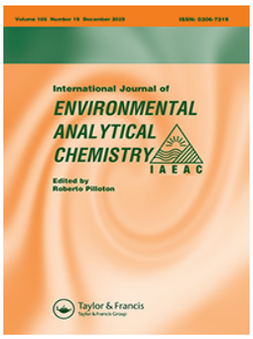

International Journal of Environmental Analytical Chemistry

ISSN: 0306-7319 (Print) 1029-0397 (Online) Journal homepage: www.tandfonline.com/journals/geac20

Mesoporous activated carbon from eggshell waste via H_3PO_4 chemical activation and its application in the removal of Janus Green B dye

Muna Abd Ul Rasool Al-Kazragi, Dhafir T.A. Al-Heetimi, Zahraa A. Al Witry & Lee D. Wilson

To cite this article: Muna Abd Ul Rasool Al-Kazragi, Dhafir T.A. Al-Heetimi, Zahraa A. Al Witry & Lee D. Wilson (24 Sep 2025): Mesoporous activated carbon from eggshell waste via H_3PO_4 chemical activation and its application in the removal of Janus Green B dye, International Journal of Environmental Analytical Chemistry, DOI: 10.1080/03067319.2025.2551743

To link to this article: https://doi.org/10.1080/03067319.2025.2551743

Published online: 24 Sep 2025.

Submit your article to this journal

Article views: 32

View related articles

View Crossmark data

Full Terms & Conditions of access and use can be found at
https://www.tandfonline.com/action/journalInformation?journalCode=geac20

INTERNATIONAL JOURNAL OF ENVIRONMENTAL ANALYTICAL CHEMISTRY
https://doi.org/10.1080/03067319.2025.2551743

Taylor & Francis
Taylor & Francis Group

Check for updates

Mesoporous activated carbon from eggshell waste via H_3PO_4 chemical activation and its application in the removal of Janus Green B dye

Muna Abd Ul Rasool Al-Kazragi[a], Dhafir T.A. Al-Heetimi[a], Zahraa A. Al Witry[a] and Lee D. Wilson[b]

[a]Department of Chemistry, University of Baghdad, College of Education for pure science Ibn-Al-Haitham, Baghdad, Iraq; [b]Department of Chemistry, University of Saskatchewan, Saskatoon, Canada

ABSTRACT

The main objective of this study was to evaluate the adsorption efficiency of two adsorbent materials, Iraqi chicken eggshells (ESh) and activated carbon (AC) derived from ESh powder for the removal of a cationic dye (Janus green B; JGD) from aqueous solution. Activated carbon was synthesised from ESh using a simple chemical activation method using phosphoric acid as the activating agent. The physicochemical properties of the adsorbents were characterised by the Brunauer–Emmett–Teller (BET) method, FT-IR spectroscopy, scanning electron microscopy (SEM), energy-dispersive X-ray spectroscopy (EDS), inductively coupled plasma optical emission spectroscopy (ICP-OES), and point of zero charge (pH_{pzc}). The results of BET analysis confirmed that AC has a higher specific surface area (4.146 m^2/g) compared to ESh (1.561 m^2/g). The effects of operational parameters including contact time (5–60 min for ESh and 5–30 min for AC), adsorbent dose (0.05–1 g/10 mL), temperature (298–318 K), and pH (3.72–11.36) were systematically investigated. Optimal adsorption occurred at pH 11.36, where JGD removal efficiencies reached 90.13% with 0.2 g/10 mL of ESh after 60 min and 92.89% with 0.1 g/10 mL of AC after 30 min at 298 K. Equilibrium data were best fitted by the Freundlich isotherm model, yielding adsorption capacities of 0.09 mg/g for ESh and 1.85 mg/g for AC at 318 K and pH 5.5. The high correlation coefficient ($R^2 = 0.99$) confirmed favourable heterogeneous adsorption. Kinetic data followed the pseudo-second-order model ($R^2 = 0.99$). Thermodynamic parameters (ΔG°, ΔH°, ΔS°) indicated that JGD adsorption onto ESh was spontaneous (ΔG°<0), exothermic (ΔH°<0), and associated with decreased randomness (ΔS°<0), while adsorption onto AC was spontaneous (ΔG°<0), endothermic (ΔH°>0), and accompanied by increased randomness (ΔS°>0). The adsorption mechanism was attributed to electrostatic interactions, hydrogen bonding, and π–π interactions. Desorption experiments demonstrated that 0.2 mol/L HNO_3 effectively regenerated both adsorbents. After seven adsorption–desorption cycles, AC exhibited superior stability and reusability compared to ESh.

ARTICLE HISTORY
Received 8 June 2025
Accepted 20 August 2025

KEYWORDS
Cationic dye; eggshell (ESh); ESh-based activated carbon; ICP-OES analysis

CONTACT Dhafir T.A. Al-Heetimi dhafir.t.a@ihcoedu.uobaghdad.edu.iq; dhafir1973@gmail.com

© 2025 Informa UK Limited, trading as Taylor & Francis Group

1. Introduction

The textile, leather, plastic, paper, and cosmetic industries all employ azo dyes, which are the most common synthetic dyestuffs [1]. They are distinguished by the presence of one or more azo (–N=N–) groups in their structure. One of the main environmental problems faced by the textile industry is the large volumes of dye-based effluent wastewater produced by its operations [2]. Numerous textile dyes are extremely hazardous to ecosystems, upon direct release into aquatic environments without proper treatment, and its long-term detrimental impacts [3]. The textile sector uses more than 10^4 tons of dyes annually, and recent estimates suggest that about 100 tons/year are discharged into aquatic habitats annually. Textile effluent frequently exhibits resistance to biodegradation due to the colourants intricate and persistent chemical composition. Due to their ability to disrupt photosynthesis and other biological processes, as well as to obstruct light transmission, dyes are visible and unwanted even at low concentrations [4]. Additionally, it has been observed that many dyes are extremely poisonous, non-biodegradable, and mutagenic, all of which have an indirect or direct effect on the health humans and ecosystems. The treatment of dye-based wastewater presents a major challenge, and several methods have been documented. *N*- or S-heteroatoms in the dye structure that are positively charged to give basic/cationic characteristics. Basic dyes are categorised as harmful colourants and exhibit a noticeable colouration even at low doses (<1 mg/L) [5]. Janus green B dye (JGD) is a water-soluble, basic (cationic) dye that finds industrial usage as a biological staining agent as well as a dye for leather, calico, cotton, and tannins. One of the well-known phenazine dyes, diethyl safranin-azo-dimethyl aniline, is present in JGD. JGD can oxidise to yield its inherent colourant qualities, adopting a range of colours from dark green to dark brown and black. It is a vital tool for scientific research because of its exceptional capacity to accurately label mitochondria in living cells. JGD is also useful for staining chromosomes, nucleic acids, sperm, yeast cells, tissue culture monolayers, and a range of tissues, such as the brain, spinal cord, and fungi [6]. When utilised medicinally, JGD surprisingly displays antimalarial properties, demonstrating its multifaceted significance in biological research and pharmaceutical applications. The symptoms of discomfort, nausea, vomiting, and diarrhoea indicate that acute exposure to JGD causes gastrointestinal and ocular issues. Additionally, cyanosis, seizures, dyspnoea, and haemoglobinuria are caused by exposure to JGD [7]. The chemical structure and characteristics of JGD are listed in Table 1. Several dye cleanup techniques have been used for common wastewater treatment, which include biological treatment, photocatalysis [8], reverse osmosis, precipitation, electrocoagulation, and ion exchange. The creation of hazardous byproducts, operational complexity, and comparatively high cost are main drawbacks of these technologies [9]. By comparison, adsorption-based treatment offers a sustainable method of decontaminating wastewater without producing any hazardous secondary byproducts. Furthermore, adsorption-based techniques entail simple unit operations with minimal startup and running expenses [10,11]. Recently, attention has been drawn to the disposal of large quantities of eggshells food waste, which result in bad odours (H_2S) and microbial growth that present environmental challenges without appropriate treatment of eggshell waste. Eggshells are a natural biomass that consists of 94% calcium carbonate, 4% organic materials, 1% calcium phosphate, and 1% magnesium carbonate. Eggshells have some disadvantages as a biosorbent due to poor sorption properties and slow

Table 1. Properties and chemical structure of JGD.

Chemical name (IUPAC)	3-Diethylamino-7-(4-dimethylaminophenylazo)-5-phenylphenazinium chloride
Synonym(s)	Diazin Green S, Union Green B
Molecular Formula	$C_{30}H_{31}ClN_6$
Molecular weight (g/mol)	511.06
Chemical structure	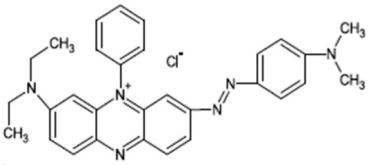
Maximum absorbance wavelength	λ_{max} = 660 nm
Melting point	160°C
Solvent solubility	Soluble in water (20 mg/ml at 20°C), and ethanol
Morphological form	Powder
Stability	Stable. Incompatible with strong oxidising agents.

kinetic processes. In this research, chemical activation method of eggshells was employed to enhance the cationic dye removal of JGD. Surface activation offers an innovative technique to generate a potential adsorbent material with improved properties. Activated carbon (AC) is a carbonaceous component that is widely consumed in the adsorption applications because of its large reactive surface area (SA) and a higher number of active functional sites. Generally, there are different activation agents, such as $MgCl_2$, NaOH, and H_3PO_4 have been employed for the activation process [12]. AC was successfully fabricated with easy chemical activation method in this paper. H_3PO_4 as strong catalytic activity is used to activate eggshells to increase their porosity, SA, and active binding groups of the adsorbent surface. Hence, it is interesting to alter ESh into AC to improve the affinity and efficiency for pollutants such as basic dyes (JGD) from aquatic systems. Besides, it can present an economical and green method for bettering the properties of adsorbents. Many low-cost biomaterials such as mango leaves [13], pine bark [14], pineapple stems [15], and casuarina empty fruit [16] are effectively for producing AC. Yönten el al. prepared AC from endemic Vitis vinifera L. grape seeds for adsorption of methyl orange from aqueous solution [17]. Chen et al. utilised mesoporous AC nano-composites from cotton fabric for efficient removal of dyes (methylene blue and methyl orange) and selective adsorption of heavy metal ions (Zn^{2+}, Cu^{2+}, Ni^{2+}, Cr^{6+} and Pb^{2+}) [18]. By using a mixture of H_3PO_4 and HNO_3-pretreated apricot stones (Djilani et al. 2015). In turn, they created AC to remove (anionic dye, methyl orange) and (cationic dye, methylene blue) [19]. In addition, agricultural waste cassava slag was applied by Wu et al. to generate AC by hydrothermal treatment to adsorb Rhodamine B from water [20]. The existence of functionalities on biomaterial surfaces, especially oxygen containing functional groups (OH, C=O, and C–O) and greater cation exchange capacity. This is one of the most promising properties of ESH and AC that provide metallic oxides and promising utility as adsorbent surfaces [21,22].

This study presents an environmentally sustainable method for dye (JGD) removal that employs raw eggshells and its modified activated carbon forms. This method is sustainable compared to conventional adsorbents. This study uniquely integrates kinetic and equilibrium models into a unified approach to provide a comprehensive evaluation of the thermodynamic parameters and adsorption properties of the materials. The effects of

several process parameters on JGD removal including contact time, initial pH, adsorbent dose and temperature were also investigated. The sustainability of the adsorption mechanism was evaluated, and a recyclability study was also conducted. This approach highlights the adsorbent's efficiency, low material cost, and environmental significance. The findings provide valuable insights into the valorisation of eco-friendly biomass waste for wastewater treatment applications.

2. Experimental

2.1. Basic dye preparation

Janus green B dye ($C_{30}H_{31}ClN_6$) was purchased from Sigma–Aldrich, its properties and chemical structure are listed in Table 1. JGD (0.5 g) was dissolved in deionised water (1 L) to make a stock solution of (500 mg/L). Working solutions (250 mL) with concentrations of 10–70 mg/L were prepared by serial dilution. All reagents in the present study were used without further purification.

2.2. Eggshell preparation

Iraqi chicken eggshells (ESh) were selected as a precursor for producing activated carbon (AC) due to their status as household waste, low cost, recyclability, and local availability in Iraq. The ESh was thoroughly washed with running tap water followed by deionised water to remove impurities and then dried under sunlight for 1 day. ESh was crushed into a powder, ground into very fine particles, sieved with a mesh size ≤75 µm, and stored in plastic containers for further use.

2.3. Preparation of activated carbon

The ESh powder was well mixed in a 4:1 weight ratio with an activating agent phosphoric acid (H_3PO_4, 98 wt.%). The mixture was dehydrated in an oven at 80°C, followed by activation in a muffle furnace at 550°C in the absence of air for 5 h. Finally, the dried material was ground and sieved to yield a particle size of ≤75 µm, and then stored in plastic containers for further use. The activated product was allowed to cool to room temperature, then washed with de-ionised water until the pH of the washing solution reached pH 7. The carbon that was produced was stored for further use, as described elsewhere [23,24].

2.4. Characterisation of eggshell powder and activated carbon

The surface charge of the ESh and AC was examined by the point of zero charge (pH_{pzc}) analysis. Dried ESh and AC samples were characterised by FT-IR spectroscopy using KBr pellets at 25°C, with a scanning speed of 0.1 cm/s. Spectra were collected over the range 4000–400 cm^{-1} employing a Shimadzu 8400 spectrophotometer (Japan). The morphology of two adsorbent surfaces was imaged by scanning electron microscopy (SEM) using the Czech version of the TE-SCAN VEG3 and energy-dispersive X-ray spectroscopy (EDS)

was conducted to characterise the ESh and AC via its composition (EDS, Hitachi, Ltd., Tokyo, Japan). A Brunauer–Emmett–Teller SA method (TriStar II Plus 2.03) to estimate specific SA and pore parameters.

2.5. Determination of point of zero charge

The pH_{pzc} determination employed the addition of 20 mL of a 0.1 M $NaCl_{(aq)}$ solution into separate 100 mL conical flasks. The desired pH was then regulated from 2.85 to 9.37 by introducing either a few drops of aqueous solution of 0.1 M HCl or NaOH into each Erlenmeyer flask. Subsequently, 0.2 g/10 mL of ESh and 0.1 g/10 mL of AC were added to each flask. The determination of the pH_{pzc} of the Esh and AC was achieved by identifying the crossover point on the plot of ΔpH against the initial pH, as outlined elsewhere [25].

2.6. Adsorption profile experiments

A batch profile was employed for a study of the JGD adsorption properties. A fixed amount of ESh and AC (0.2 and 0.1 g/10 mL) were put separately in a serial conical flask (100 mL) containing (10 mL) of JGD solution with an initial JGD concentration (50 mg/L). The flasks were placed in a thermostatic water bath to be stirred at a set shaking speed of 150 rpm at 298 K until equilibrium was attained. The adsorption process was performed by evaluating a number of parameters, such as (ESh and AC) dose (0.05–0.8 g/10mL), pH (2.85–9.37), initial JGD concentration (10–70 mg/L) and variable temperature (298–318 K) three replicates. To adjust the pH of the JGD solution, 0.1 M HCl or 0.1 M NaOH was used. After the adsorption process, the mixtures were centrifuged (Hettich EBA-20, Germany, 6,000 rpm) at 3,000 rpm for 5 min. Before analysis, the resultant supernatant was filtered using No. 42 filter paper. The absorbance of filtrated samples was measured by UV-VIS spectrophotometer with a double-beam type (*T*-80, England) with a maximum wavelength, λ_{max} of 660 nm. Equation (1) and (2) were used to compute the JGD removal (JR; %) and the adsorbed capacity (Q_{eq}) at equilibrium, respectively.

$$JR\% = \frac{C_{in} - C_{eq}}{C_{in}} \times 100\% \tag{1}$$

$$\frac{Q_{eq} = \left(C_{in} - C_{eq}\right) \times V_{sol}}{W_t} \tag{2}$$

Where C_{eq} (mg/L), C_{in} (mg/L), V_{sol} (L), and W_t (g/L) represent the concentration of JGD at equilibrium, initial JGD concentration, volume of JGD solution and weight of the ESh and AC, respectively.

Desorption study was also illustrated by the batch method with similar adsorption experiments, where 50 mL of JGD solution with a starting concentration of 50 mg/L was added with (0.2 and 0.1 g/L) of Esh and AC, respectively, under optimal external conditions (pH 5.5, equilibrium time of 60 min for ESh and 30 min for AC, 298 K, and a fixed shaking speed of 150 rpm) for seven repetition runs. At equilibrium, the biosurfaces of ESh and AC were cleaned with deionised water to remove the unwanted JGD cations. The

saturated bioadsorbents were then treated with 50 mL of HNO_3 (0.2 mol/L) as a desorbing agent. A series of (7) continuous cycles were accomplished to evaluate the samples were reusable.

3. Results and discussion

3.1. Characterisation of ESh and AC

3.1.1. FTIR analysis

The FTIR results for ESh, as illustrated in Figure 1(a), reveal a broad band at 3310 cm^{-1} is attributed to the hydroxyl stretching vibrations. The weak bands at 2921 and 2873 cm^{-1}

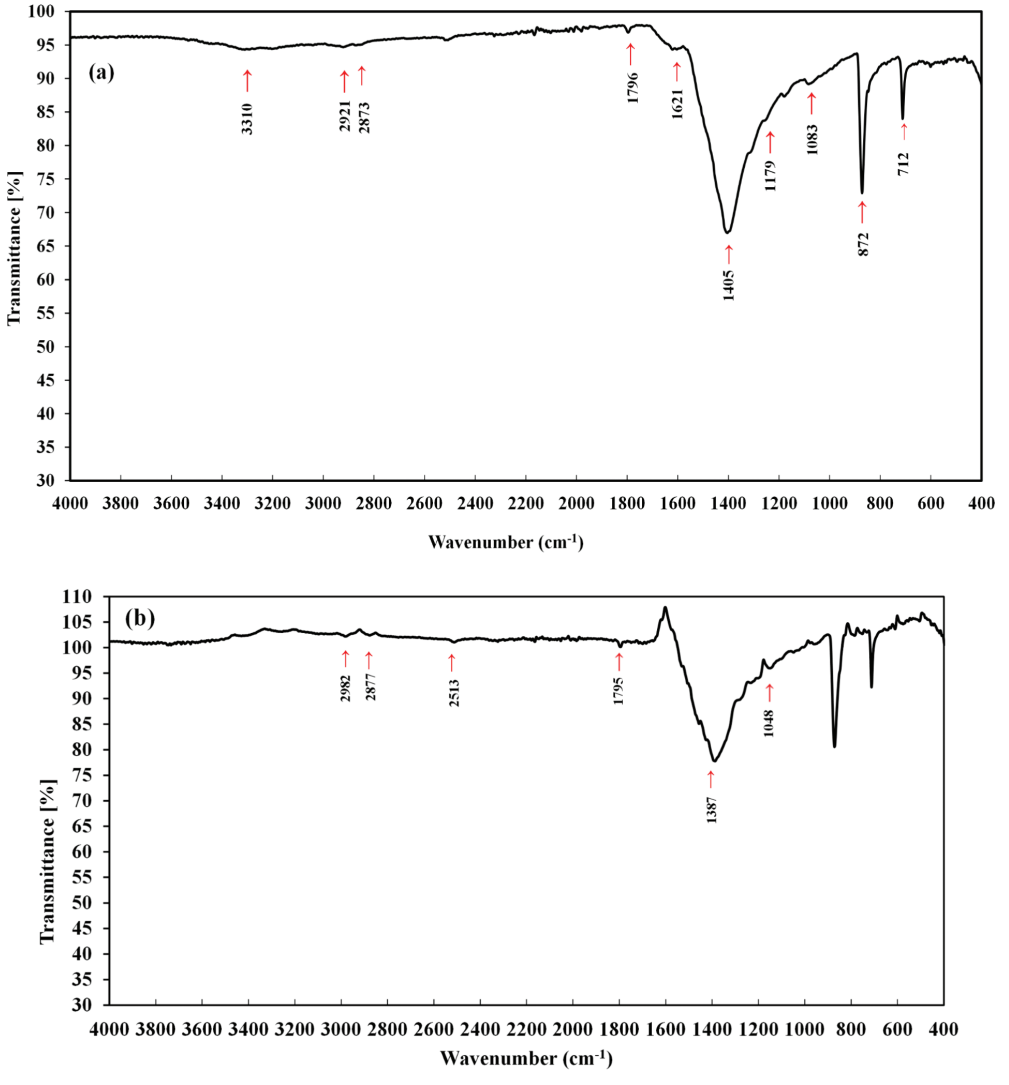

Figure 1. (a) FTIR spectra of ESh in transmittance (%) mode (b) FTIR spectra of AC in transmittance (%) mode.

are assigned to the aliphatic C–H stretching of (methyl and methylene groups). The band at 1621 cm^{-1} relates to C=O vibrations, while the FTIR bands at 1179 and 1083 cm^{-1} are assigned to a C–O bond. The weak band at 1796 cm^{-1} corresponds to the C=O bonds of carbonates in ESh. The band at 712 cm^{-1} is attributed to the Ca–O bond. Additionally, the bands at 1405 cm^{-1} and 872 cm^{-1} correspond to the C–O bond stretching and bending vibrations in ($CaCO_3$), respectively. After activation of ESh by H_3PO_4, the FTIR spectrum of the AC adsorbent in Figure 1(b) accounts for the most common functional groups of AC as represented by weak bands near 2982 and 2877 cm^{-1}, which support the presence of the C–H bond of alkane groups. The FTIR band observed at 2513 cm^{-1} is assigned to the O=C=O stretching vibration. The band at 1621 cm^{-1} in the ESh spectrum moved to higher wavenumber (1795 cm^{-1}). Additionally, the band at (1083 cm^{-1}) slight shifted to 1048 cm^{-1}, which confirms successful activation of ESh by phosphoric acid into AC. The bands 1387 cm^{-1} related to the C=C stretches of carbon–carbon alkene bonds [26,27]. The FTIR band at 2513 cm^{-1} supports the presence of an alkyne (C≡C) bond [28].

3.1.2. SEM-EDS analysis

Figure 2(a,b) depicts the SEM images of the ESh and AC surfaces. It can be seen in Figure 2 (a) that the ESh surface appears to be a rugged material with rough texture, cracks, voids and a porous structure, where surface irregularities such as tubular holes are distributed throughout [29]. Upon activation of the ESh powder by H_3PO_4 Figure 2(b), the AC surface became smoother in appearance, where many outer and interior pores of various size and shape were clearly observed along the AC surface. Since AC is a highly porous material, the presence of surface pores offers advantages because it can provide more sites for JGD adsorption on the external and internal surface structure. The macropores are easily visible, facilitating the simple diffusion of a huge number of JGD cations into the pore structure and the adsorption of dye species onto the AC surface [19].

EDS examination of ESh Figure 3(a) indicates that the surface is composed of 42.67% (O), 9.97% (C), 47.03% (Ca), 0.18% (Mg) and 0.16% (P). However, after activation with H_3PO_4 Figure 3(b) the composition changed to 40.89% (O), 15.02% (C), 40.94% (Ca), 0.28% (Mg) and 0.09% (P) The EDS spectra illustrate a notable rise in C and Mg content (%), whereas a reduction in O, Ca, and P (%) is also noted.

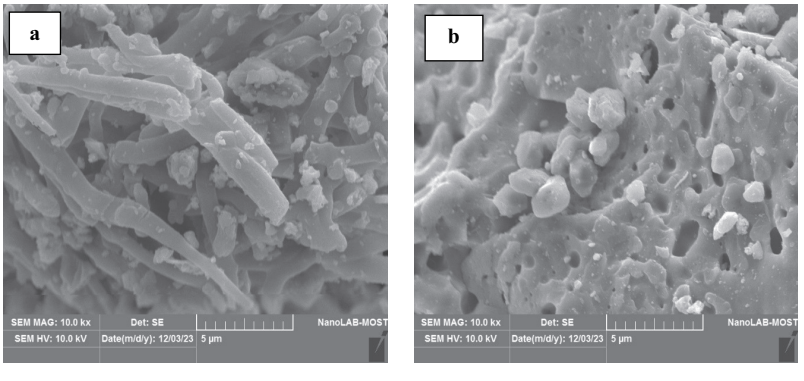

Figure 2. SEM images of (a) ESh and (b) AC.

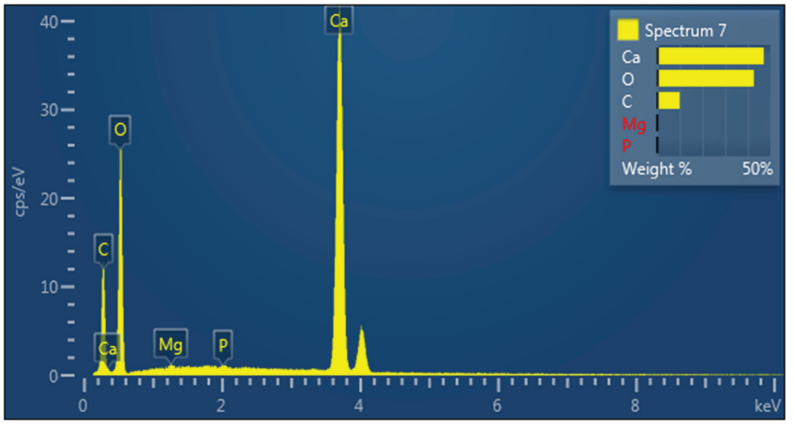

(a)

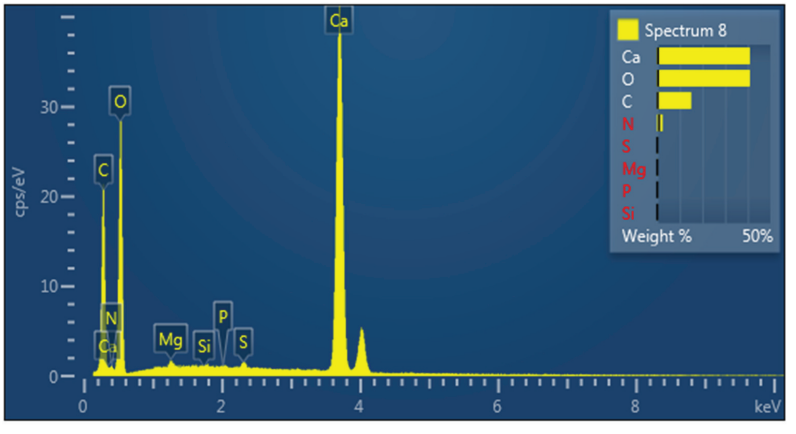

(b)

Figure 3. EDS analysis of (a) ESh and (b) AC.

3.1.3. BET and surface area analysis

Figure 4(a,b) depicts the N_2 adsorption-desorption isotherms and BET analysis plots for ESh and AC. Based on the results of the BET analysis, the specific SA, pore volume and mean pore diameter values for ESh were found to be 1.561 m^2/g, 0.0002 $cm^3\ g^{-1}$ and 16.04 nm, respectively. For AC, the corresponding values were 4.146 m^2/g, 0.001 $cm^3\ g^{-1}$ and 9.53 nm. The results revealed that AC has greater specific area, total pore volume, and smaller pore sizes than ESh. Furthermore, according to IUPAC classification, the two adsorbents exhibited mesoporous structures [30].

3.1.4. ICP-OES analysis

Measurements of the atomic composition of particular ESh and AC samples were identified using inductively coupled plasma mass spectrometry (ICP-MS) as listed in Table 2. The observations support the presence of major and minor elements on the adsorbent surfaces as revealed by wt.-based composition (ppm).

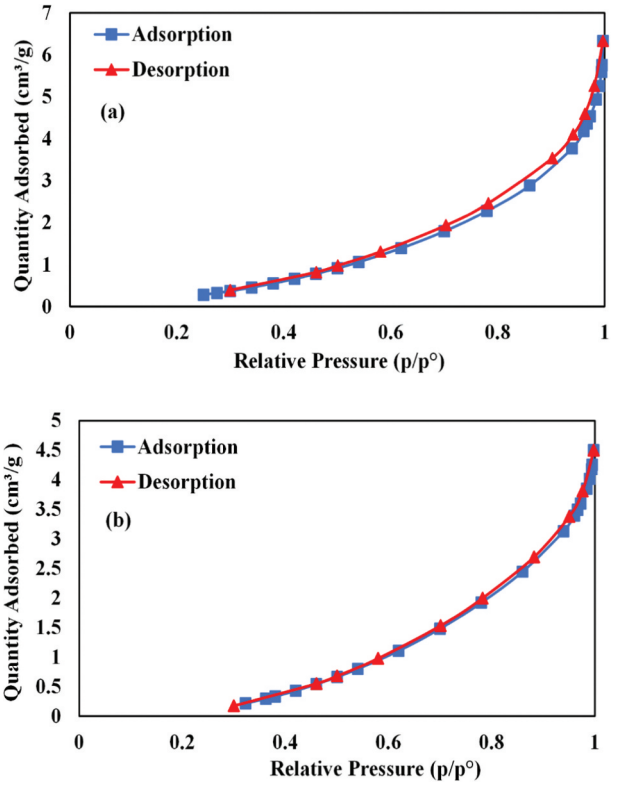

Figure 4. N_2 adsorption-desorption isotherms of (a) ESh and (b) AC.

Table 2. Elemental content (W_t, ppm) of ESh and AC as determined by ICP-OES analysis.

Esh		AC	
Element	W_t (ppm)	Element	W_t (ppm)
Cd	0	Cd	2.7
As	0.9	Co	2.85
B	0.15	Cr	0.15
Bi	0.75	Bi	0.6
Cu	0.15	Cu	2.7
Fe	0.45	Fe	0.15
K	6.75	K	19.5
Li	1.2	Li	6.75
Mg	81.6	Mg	59.1
Ca	Over range	Ca	Over range
Na	80.4	Na	54.15
Ni	2.25	Ni	0.15
In	7.2	In	0.45
Se	5.1	Se	0.75
V	0.45	V	0.75
Zn	125	Zn	0.15
Mn	0.00	Mn	0.45
Hg	1.5	Hg	0.6

3.2. Adsorption parameter study of the JGD adsorption process

3.2.1. Influence of adsorbent dose

Variable amounts of ESh and AC adsorbents, ranging from 0.05 to 0.8 g/10 mL at constant solution volumes (10 mL), were used to account for the impact of ESh and AC dosage for the removal of the JGD from aqueous media, where the initial concentration (JGD) was 50 mg/L. The primary JGD solution's natural pH was set at 5.5, contact times for ESh and AC were 60 min and 30 min, respectively, and other experimental settings were maintained at 298 K and 150 rpm for the shaking speed. Figure 5 shows the results, where the level of JGD (%) removal by ESh decreased as the adsorbent dose increased, attributed to a greater number of unsaturated adsorption sites [31]. However, the observed increase in the RE% of JGD with incremental AC dosage relates to an increase in the available adsorbent SA, as the number of active sites increase. According to these results the optimal dosage values for effective JGD removal are 0.2 g/10 mL for ESh and 0.1 g/10 mL for AC, which allow for efficient treatment with minimal adsorbent usage. Hereafter, 0.2 and 0.1 g/10 mL were chosen as an optimum ESh and AC dosage for this adsorption study [5,32].

3.2.2. Influence of contact time

Figure 6 demonstrates how the contact time affects the adsorption capacity of the JGD onto ESh and AC. By varying the duration of contact time between 5 min to 60 min. The JGD uptake was rapid at the initial stage until it reached equilibrium at a contact time of ca. 60 min for ESh and ca. 30 min for AC. Initially, the adsorption rate was rapid as the outer surface sites of the sorbents were available active sites for JGD adsorption. Upon saturation of the surface sites, the JGD dye species bind with the inner pores of the adsorbent, as evidenced by a decreased adsorption rate [4].

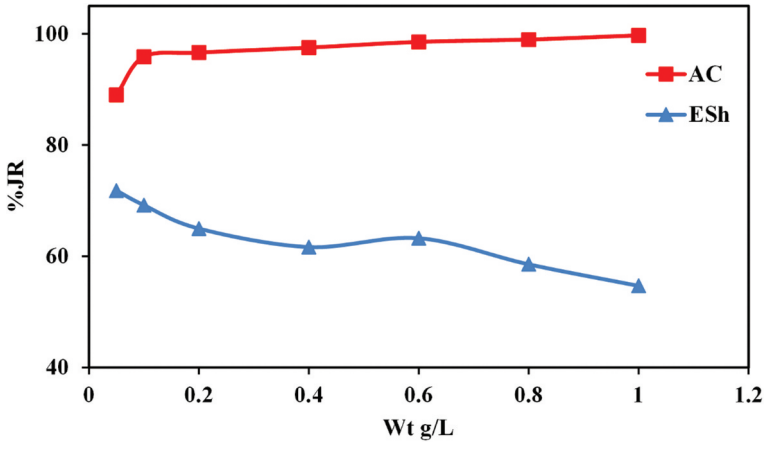

Figure 5. The influence of adsorbent surface dose on the removal of JGD onto ESh and AC at 298 K, JGD conc.=50 mg/L, shaking speed= 150 rpm, pH= 5.5, and t for ESh and AC = 60 min and 30 min, respectively.

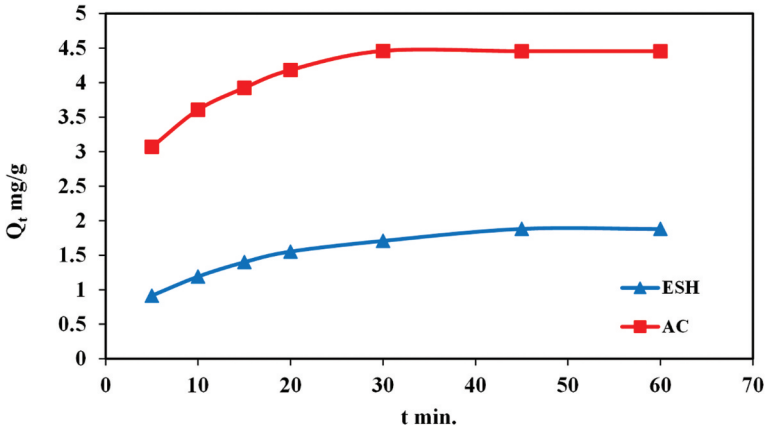

Figure 6. The influence of contact time on the adsorption capacity of JGD onto ESh and AC at 298 K, JGD conc.=50 mg/L, shaking speed= 150 rpm, pH= 5.5, and ESh and AC dose = 0.2 and 0.1 g/10 mL, respectively.

3.2.3. Influence of pH and pH_{PZC}

Dye removal is often affected by the solution pH since the pH of the medium affects the adsorbent surface charge, since the functional adsorbent groups may undergo variable ionisation at variable pH. Considering the results related to pH_{PZC} and the impact of the initial pH on the JR% tested profile shown in Figure 7(a–b) at variable pH. Figure 7(a) reveals that the JR% onto ESh and AC increased as the pH varied from 3.72 to 11.36. In order to support the experimental results, the pH_{PZC} for ESh and AC are equal to 5.3 and 6.1, respectively, Figure 7(b). At pH_{PZC}, the adsorbent surfaces are affected similarly by positive and negative charged adsorbates equally. As the pH decreases ($pH < pH_{PZC}$), the adsorbent surfaces become positively charged due to the adsorption of hydrogen ions, and the JR% decreases. At greater pH ($pH_{PZC} < pH$), the adsorbent surfaces are negatively charged and a strong electrostatic attraction occurs between the cationic JGD species and the negative surface sites on the ESh and AC surfaces, resulting in enhanced dye removal (JR; %) of JGD [33].

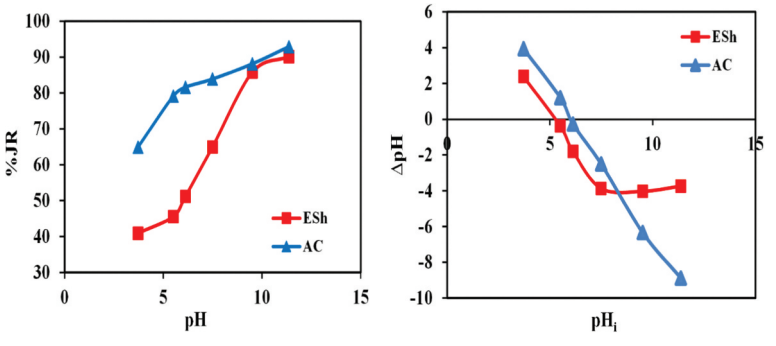

Figure 7. (a) Influence of pH solution on the removal of JGD onto ESh and AC surfaces and (b) pH_{pzc} of ESh and AC surfaces at 298 K, JGD conc.=50 mg/L, shaking speed= 150 rpm, ESh and AC dose = 0.2 and 0.1 g/10 mL, and t for ESh and AC = 60 min and 30 min, respectively.

3.2.4. JGD adsorption kinetics

The study of adsorption kinetics provides insight on the adsorption mechanism and the mode of transport of solute from one phase to another. In order to account for the kinetic profiles, two models are suggested like the Lagergren model (also known as the pseudo-first-order model, PO1) and (the pseudo-second-order model, PO2) [34]. The coefficient (R^2) was determined in order to assess the two models' goodness-of-fit and applicability.

The linear form of PO1 kinetic model is presented by the Lagergren equation [35].

$$\ln\left(Q_{eq} - Q_t\right) = \ln Q_{eq} - k_1\, t \tag{3}$$

Ho and Mckay described the PO2 kinetic, where the kinetic rate expression is represented, as follows [36]:

$$\frac{t}{Q_t} = \frac{1}{k_2\, Q_{eq}^2} + \frac{t}{Q_{eq}} \tag{4}$$

Where, k_1 (min^{-1}) and k_2 (g/mg min) represent the adsorption rate constants, while Q_{eq} and Q_t (mg/g) are the adsorption capacity of the JGD adsorbed at equilibrium and at any time (t, min) over the adsorption profile. These parameters (Q_{eq}, k_1, and k_2) can be calculated experimentally by plotting $\ln(Q_{eq} - Q_t)$ vs. t Figure 8(a,b) and (t/Q_t) vs. t Figure 9(a,b), respectively. For the two prepared adsorbents under study, the adsorption of JGD agreed with the PO2 kinetic profile with R^2 closer to 0.99 (Table 3). Moreover, the calculated equilibrium adsorption capacities (Q_{eq}, cal) of the pseudo-second-order kinetics model were closer to the actual (Q_{eq}, exp) [37].

3.2.5. Activation energy of JGD adsorption

The activation energy of the adsorption profile, which represents the minimal energy that reactants must retain in order for the reaction to proceed, was evaluated by employing the Arrhenius equation. As shown in Figure 10, this equation accounts for the link between the PO2 rate constant (k_2) and the investigated temperatures to account for the energy of activation (E_a) at the adsorbent surface.

$$\ln k_2 = \ln A - \frac{E_a}{RT} \tag{5}$$

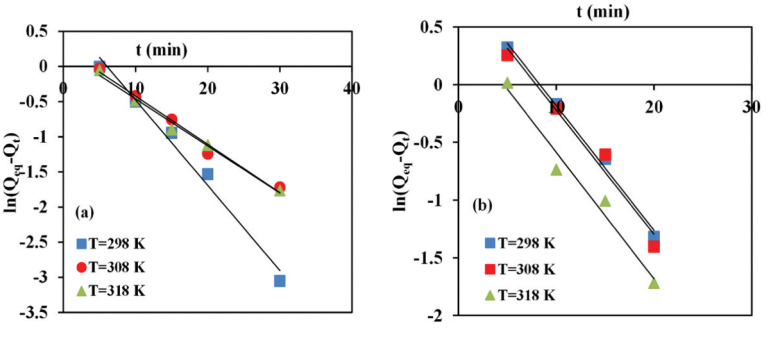

Figure 8. Linear plot of the pseudo-first-order kinetics model (PO1) for JGD dye adsorption onto (a) ESh and (b) AC at different temperatures.

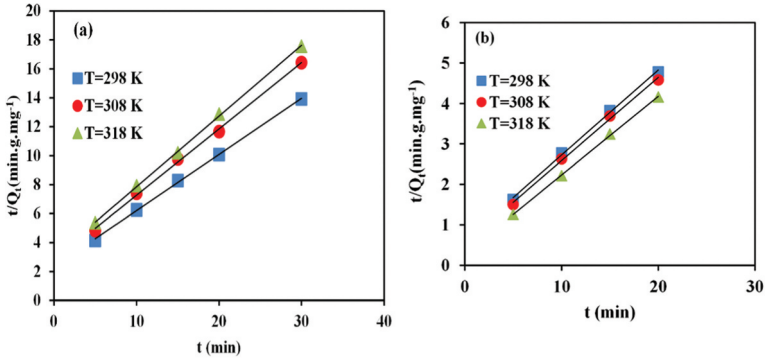

Figure 9. Linear plots of the pseudo-second-order kinetics model for JGD dye adsorption onto (a) ESh and (b) AC at different temperatures.

Table 3. Kinetics parameters for the adsorption of JGD onto ESh and BAC surfaces (C_o = 50 mg/L, shaking speed = 150 rpm, pH = 5.5, ESh and AC dose = 0.2 and 0.1 g/10 mL, and t for ESh and AC = 60 min and 30 min, respectively).

		Pseudo-first-order				Pseudo-second-order		
Adsorbent	T (K)	k_1 (min^{-1})	$Q_{eq(exp)}$ (mg/g)	$Q_{eq(cal)}$ (mg/g)	R^2	k_2 (g/mg min)	$Q_{eq(cal)}$ (mg/g)	R^2
ESh	298	0.121	2.155	2.080	0.9846	0.065	2.574	0.9994
	308	0.069	1.826	1.302	0.9857	0.078	2.185	0.9984
	318	0.067	1.709	1.232	0.9894	0.080	2.049	0.9996
AC	298	0.108	4.183	2.452	0.9926	0.168	4.760	0.9985
	308	0.107	4.366	2.344	0.9738	0.193	4.861	0.9973
	318	0.120	4.810	1.663	0.9722	0.337	5.141	0.9995

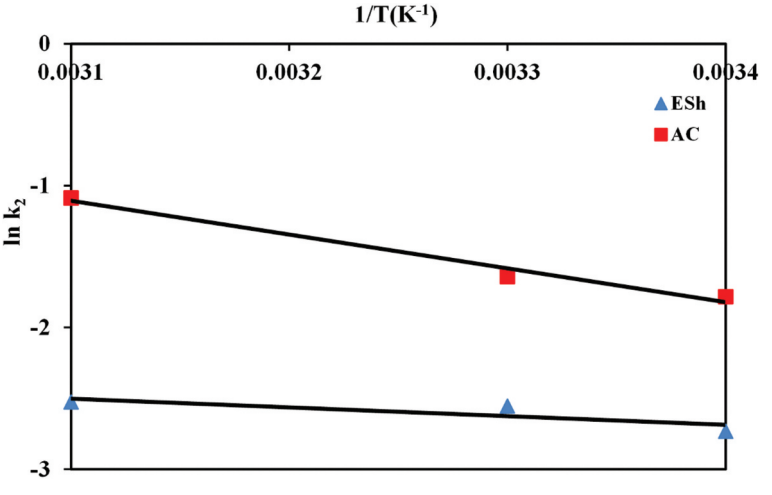

Figure 10. Plot of ln k_2 vs. 1/T for determination of activation energy at various temperatures.

In this context, k_2 represents the rate constant obtained from the PO2 profile, E_a is the Arrhenius activation energy, A is the pre-exponential or frequency factor, R is the universal gas constant (8.314 J/mol K), and T is the absolute temperature. According to the van't Hoff plots shown by Equation (5), the linear dependence yields a straight line with slope ($-E_a/R$) that enables estimation of E_a. The magnitude of E_a gives an idea of a kind of adsorption, which may be either physical or chemical in nature. The physisorption mechanism concurs with E_a between 5 and 40 kJ/mol, whereas chemisorption corresponds to a higher range of E_a values (40–800 kJ/mol). The estimated activation energy (8.22 and 27.23 kJ/mol) obtained for ESh and AC supports that JGD adsorption onto ESh and AC surfaces is physisorption in nature [5].

3.2.6. Isotherm modeling

Adsorption isotherms provide insight as to the nature of the adsorption process. The influence of the starting concentration of JGD enables determination of the relevant isotherm model to describe the experimental adsorption profile. The Langmuir [38], Freundlich [39] and Temkin [40] isotherms were employed to assess the experimental profiles as a function of concentration. If the value of the correlation coefficient (R^2) is close to a unitary value, an acceptable goodness-of-fit is concluded.

The Langmuir model was developed to describe monolayer formation onto a surface holding a definite number of active sites during the adsorption process, the adsorbent surface is homogeneous with no migration of the adsorbate particles in the plane of the adsorbent surface. The linear form of Langmuir isotherm is expressed by Equation (6):

$$\frac{C_{eq}}{Q_{eq}} = \frac{1}{K_L Q_{max}} + \frac{C_{eq}}{Q_{max}} \tag{6}$$

The Freundlich model presumes a multilayer formation of adsorbate species onto non-homogeneous surface with distinguished adsorption energy sharing. The linearised form of Freundlich isotherm is defined by Equation (7):

$$\log Q_{eq} = \log K_F + \frac{1}{n} \log C_{eq} \tag{7}$$

The Temkin model deliberated adsorbate-adsorbent interaction on the non-homogeneous surface and the binding energy of adsorption system is evenly dispersed up to maximal binding energy. The heat of adsorption diminishes linearly with adsorbent surface coverage. The linear form of Temkin model is stated by Equation (8):

$$Q_{eq} = B \ln A_T + B \ln C_{eq} \tag{8}$$

C_{eq} represents equilibrium concentration of JGD (mg/L), while Q_{eq} and Q_{max} are the JGD adsorption capacity and the maximum monolayer adsorption capacity in (mg/g), respectively, K_L is the Langmuir constant (L/mg) that is connected to adsorption energy. A Langmuir plot of C_{eq}/Q_{eq} vs. C_{eq} is presented in Figure 11(a,b). The Langmuir parameters K_L and Q_{max} were estimated using the intercept and slope parameters. K_F is the Freundlich isotherm constant (mg/g), which relates to the adsorption capacity, according to the Freundlich adsorption intensity (1/n). The Freundlich model was plotted as a log–log plot for log Q_{eq} against log C_{eq} in Figure 12(a,b). In Equation (8), the value of B equals (RT/b), where b signifies the

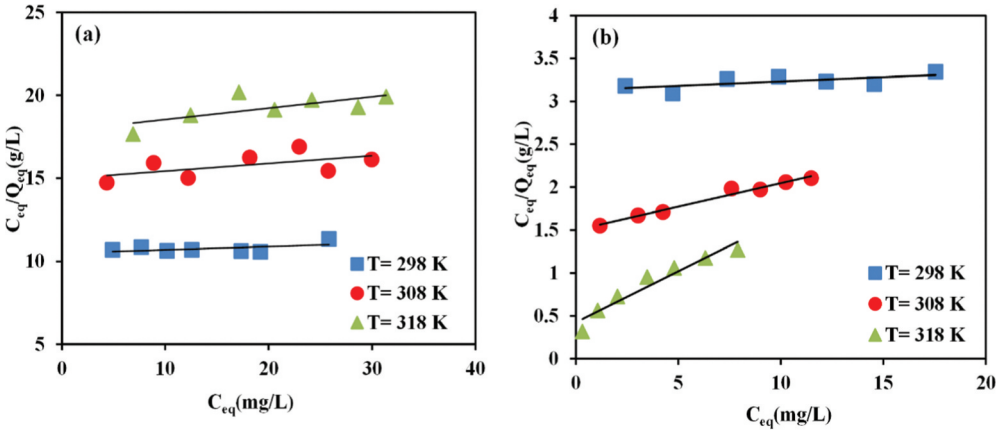

Figure 11. Langmuir isotherm plots for JGD adsorption by (a) ESh and (b) AC.

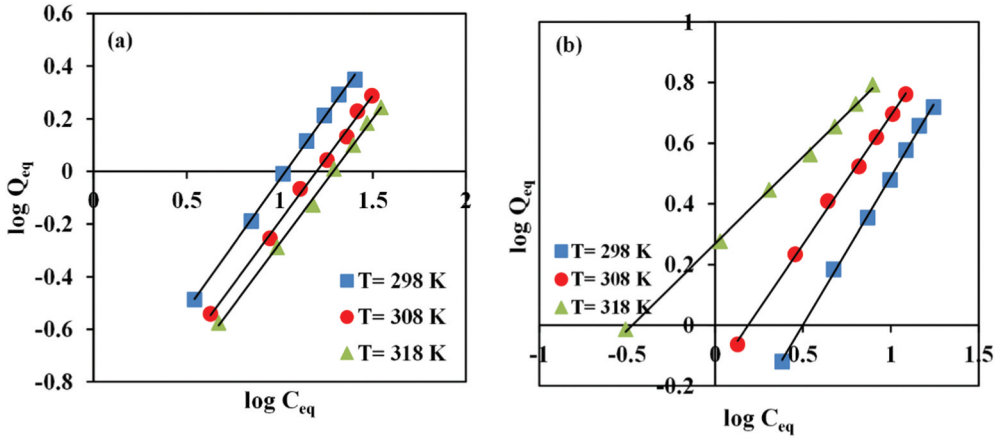

Figure 12. Freundlich isotherm plots for JGD adsorption by (a) ESh and (b) AC.

Temkin constant that corresponds to adsorption energy (J/mol), A_T denotes the Temkin model constant (L/g), R is the gas constant (8.314 J/mol K), and T is absolute temperature. The values of (B and A_T) being accounted from the slope and intercept of the graph of Q_{eq} against ln C_{eq}. A Temkin profile was illustrated by Q_{eq} vs. ln C_{eq} in Figure 13(a,b). The detailed factors of three isotherms and the coefficients of determination (R^2) are summarised in Table 4. The value of R^2 for the Freundlich isotherm exceeds that of the Langmuir and Temkin isotherms, which supports that the Freundlich provides a better account of the adsorption profile of JGD by the ESh and AC systems. This indicates that JGD removal is heterogeneous and/or multilayer in nature. Moreover, the value of (1/n) for both adsorbents was below 1, which indicates that the trend of JGD adsorption by ESh and AC was favourable at the conditions employed [31]. Table 5 compares the Q_{max} of ESh and AC with previous researches for variable dyes removal by other adsorbents stated in literature.

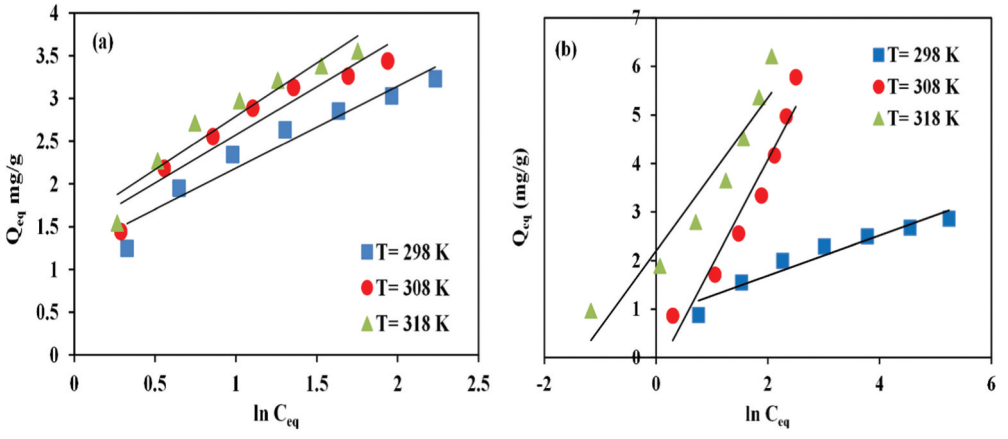

Figure 13. Temkin isotherm plots for JGD adsorption by (a) ESh and (b) AC.

Table 4. Model factors of linearised Langmuir, Freundlich and Temkin isotherms for JGD adsorption onto ESh and AC (shaking speed = 150 rpm, pH = 5.5, ESh and AC dose = 0.2 and 0.1 g1/10 mL, and t for ESh and AC = 60 min and 30 min, respectively).

		Langmuir			Freundlich			Temkin		
Adsorbent	T (K)	K_L (L/mg)	Q_{max} (mg/g)	R^2	K_F (mg/g)	1/n	R^2	B (J/mol)	A_T (L/g)	R^2
ESh	298	0.0018	50.8	0.2853	0.0953	0.9893	0.9988	0.9607	3.4628	0.9371
	308	0.0031	21.6	0.3342	0.0713	0.9567	0.9970	1.1272	3.4867	0.9169
	318	0.0038	14.6	0.4992	0.0600	0.9487	0.9984	1.2479	3.3616	0.9186
AC	298	0.0031	100.0	0.4394	0.3250	0.9771	0.9992	0.4146	5.6298	0.9305
	308	0.0364	18.3	0.9774	0.6892	0.8528	0.9983	0.4289	1.4542	0.9383
	318	0.2784	8.4	0.9302	1.8556	0.5714	0.9989	0.5813	0.1256	0.9180

Table 5. Comparison of Q_{max} for different biosorbents for dyes adsorption.

Adsorbent	pollutant	Q_{max}(mg/g)	pH	Dose (g/L)	Reference
Ac derived from rice husk	Janus green B	2.00	2.0	13.0	[41]
Coconut shell charcoal	Cationic red colour 14	22.93	6.0	4.2	[42]
Pistachio shells	Janus green B	3.60	7.0	1.5	[43]
Bivalve shells	Methylyene blue	1.00	10.4	1.0	[44]
thermal activation of banana peels (AMP)	Janus green B	1.10	7.0	0.01	[45]
ESh	Janus green B	0.09	5.5	0.2	Present work
Ac derived from egg shell	Janus green B	1.85	5.5	0.1	Present work

3.2.7. Error analysis

An error function model is used to assess the appropriateness of isotherm profile with the empirical data, error function (coefficient of nondetermination) was accounted by the following equation [46].

$$Coefficient\ of\ nondetermination = 1.000 - R^2 \tag{9}$$

Here, R^2 is represented the coefficient of determination which is estimated from isotherm models. The coefficient of nondetermination data tabulated in Table 6 imply that the Freundlich model provides an excellent model of the adsorption process.

Table 6. Error analysis for various isotherm model at variable temperature values.

Adsorbent	Isotherm	T= 298 K	T= 308 K	T= 318 K
ESh	Langmuir	0.7147	0.6658	0.5008
	Freundlich	0.0012	0.0030	0.0016
	Temkin	0.0629	0.0831	0.0814
AC	Langmuir	0.5606	0.0226	0.0698
	Freundlich	0.0008	0.0017	0.0011
	Temkin	0.0695	0.0617	0.0820

3.2.8. Thermodynamic equilibrium analysis

Adsorption thermodynamic parameters reveal the energetics that favour the adsorption process. The temperature variation data of JGD adsorption was carried out to account for thermodynamic parameters like the differences of standard Gibbs free energy, enthalpy, and entropy at 298, 308, and 318 K. The following are the Equation (10–12) [47]:

Gibbs free energy differences (J/mol):

$$\Delta G^{\circ} = -RT\ \mathrm{In}\ K_d \tag{10}$$

where K_d is the distribution coefficient defined by Equation (11):

$$K_d = \frac{(C_{in} - C_{eq})}{C_{in}} \times \frac{V}{Wt} \tag{11}$$

The difference in standard entropy and enthalpy differences are related by Equation (12):

$$\mathrm{In}K_d = \frac{\Delta S^{\circ}}{R} - \frac{\Delta H^{\circ}}{RT} \tag{12}$$

Where Q_{eq} is the JGD adsorption capacity in (mg/g), C_{eq} represents JGD equilibrium concentration (mg/L), R (8.314 J/mol K) is the universal gas constant and T is the absolute temperature (K). The magnitudes of ΔH° and ΔS° were estimated from the slope and intercept terms of the van't Hoff plot (ln K_d vs. 1/T) for each adsorbent system, as shown in Figure 14. Table 7 lists the experimental results of thermodynamic factors for JGD adsorption using ESh and AC surfaces. For both systems (ESh and AC), the negative ΔG°

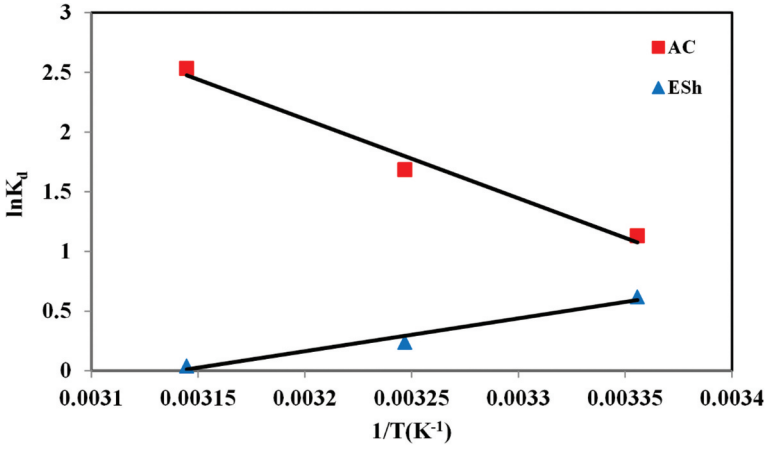

Figure 14. ln K_d vs 1/T plot for the adsorption of JGD by ESh and AC.

Table 7. Thermodynamic parameters for the adsorption of JGD onto ESh and AC.

Adsorbent	T (K)	ln K_d	ΔG^o(J/mol)	ΔH^o(kJ/mol)	ΔS^o (J/mol K)
ESh	298	0.6188	−1533	−22.89	−71.89
	308	0.2388	−611.7		
	318	0.0395	−104.4		
AC	298	1.1307	−2801	+55.11	+193.9
	308	1.6855	−4316		
	318	2.5333	−6698		

values for the experimental range of temperature ranges indicated these trends were spontaneous and feasible [37,47,48]. For the ESh system, the rise in ΔG° with incremental temperature records indicate that the adsorption of JGD onto ESh surface is favourable at low temperatures, while the ΔG° signs declined with the rise in temperatures indicating that the profile adsorption of JGD onto AC was more spontaneous with temperature. The negative sign of ΔH° supports that the adsorption process of JGD by ESh is exothermic, whereas a positive sign of ΔH° indicates that an endothermic process for AC. The decreasing randomness at the ESh surface during the adsorption of JGD concurs with the negative sign of ΔS° [49]. On the other hand, the positive sign of ΔS^o indicates a rise in entropy during the adsorption of JGD onto AC. JGD ions and solvent on the surface of AC are inferred to be in a more ordered state prior to the adsorption process. Therefore, as the adsorption process progresses, the rotational distribution and translational energy increase, leading to a positive entropy value and greater randomness at the solid–liquid interface [50].

3.3. Adsorption mechanism

Multiple mechanisms have been proposed for the removal of organic dyes from aqueous systems, such as hydrogen bonding, hydrophobic interactions, π-π electron-donor-acceptor interaction, and electrostatic attraction [51]. In Figure 15, Janus Green B (JGD) can interact with the adsorbent surfaces of ESh and AC in three possible ways: (1) electrostatic attraction, (2) π–π interaction, and (3) H-bonding. The presence of abundant oxygen-containing functional groups supplies a negative charge on two surfaces, which facilitates the electrostatic interaction of ESh and AC with positively charged JGD cations. Electrostatic attraction between the ($-N^+$) groups of JGD and the negatively charged surface groups such as –OH, C=O, –C–O, O=C=O, and –COOR of ESh and AC may act as the essential adsorption mechanism. In addition, π–π interactions means (Hydrophobic, Pi-Pi Stacked and Pi-Pi T-shaped) may occur between the localised π-electrons in the aromatic rings of JGD and those in the conjugated carbon–carbon double and triple bonds (C=C, C≡C) of the AC surface. Adsorption may occur as a result of H-bonding (Pi-Donor) between the H-containing groups of JGD cations and the O-containing groups of ESh or AC, and vice versa. The produced AC in this study shows a comparatively greater adsorption capability than Esh [52,53].

3.4. Desorption and regeneration of ESh and AC

The recyclability was an essential feature of the biosorbents. In this study, the best outcomes were obtained with HNO_3 (0.2 mol/L) for regeneration of ESh and AC after

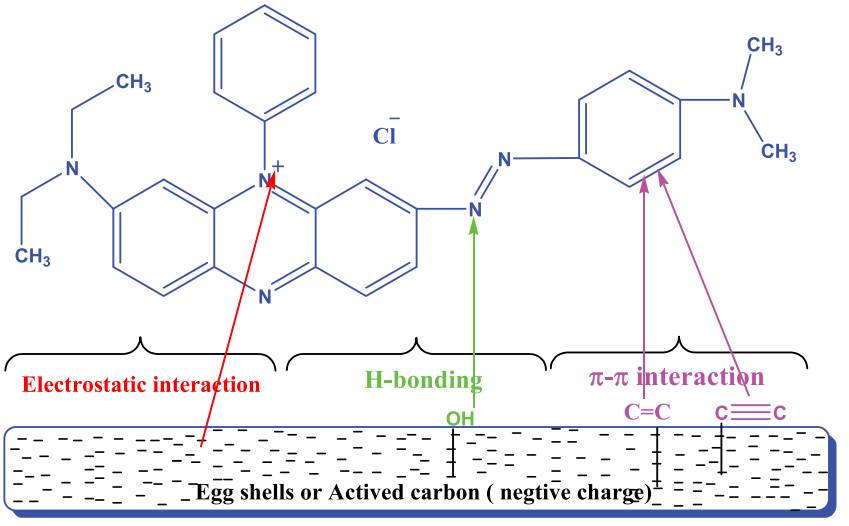

Figure 15. The adsorption mechanism between ESh and AC surfaces with JGD.

JGD adsorption. Figure 16, presents the reduction in removal efficiency (%) from 84.89% (cycle 1) to 14.55% (cycle 7) and 94.27% (cycle 1) to 36.75% (cycle 7) for ESh and AC, respectively. The mechanism of desorption process may be related to the presence of weak electrostatic forces between JGD and both adsorbent surfaces. Furthermore, the low removal efficiency (%) may occur due to the protonation of ESh and AC with an acidic eluent. The removal efficiency (%) of AC was diminished more than ESh. This result indicates the high stability and reuse because of the easy and energetic separation of the biomaterials [2,54].

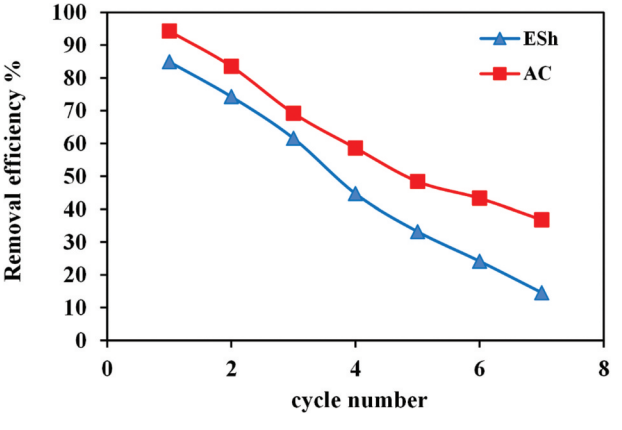

Figure 16. Influence of regeneration run on the removal efficiency % of JGD by ESh and AC. C_o = 50 mg/L, shaking speed= 150 rpm, pH= 5.5, ESh and AC dose = 0.2 and 0.1 g/10 mL, and t for ESh and AC = 60 min and 30 min, respectively.

4. Conclusion

This study focused on a comparative evaluation of raw biomass (Iraqi chicken eggshells) and activated carbon derived from it for the adsorption of the toxic dye (JGD) from aqueous solution. The chemical activation of ESh was performed with H_3PO_4. The SA of ESh was 1.561 m^2/g that increased to 4.146 m^2/g after chemical activation with H_3PO_4.The optimum conditions for accomplishing the high removal efficiency (90.13% for ESh) and (92.89% for AC) were identified as a pH of 11.36, an initial JGD concentration of 50 mg/L, a contact times of 60 min and 30 min and an adsorbent weights dosages of 0.2 g/10 mL and 0.1 g/10 mL for ESh and AC, respectively. The adsorption results of both adsorbent surfaces were suitably described by the Freundlich isotherm equation. The adsorption capacities values were found to be (0.09 mg/g) for ESh and (1.85 mg/g) for AC. Furthermore, the kinetic investigation proved that the experimental result was well modelled by PO2. The higher correlation coefficient (R^2, 0.99) and error deviation magnitudes (coefficient of nondetermination) with respect to the experimental results proved that the biosorption systems of JGD onto ESh and AC could be depicted by the Freundlich profile. Desorption mode revealed 14.55% ESh and 36.75% AC recovery with (0.2 mol/L) HNO_3 after seven runs. Thermodynamic data viz. (ΔG°, ΔH°, and ΔS°) shows negative values of ΔG° (−1533, −611.7, and −104.4 J/mol), ΔH° (−22.89 kJ/mol), and ΔS° (−71.89 J/mol.K) suggesting that the adsorption of JGD by ESh feasibility, exothermic character, and diminishing randomness on the ESh surface. On the contrary, the positive values of ΔH° (+193.9 kJ/mol) and ΔS° (+55.11 J/mol.K) highlight endothermic nature of the biosorption of JGD by AC and greater molecular disorder after JGD biosorption, where negative values of ΔG° (−2801, −4316, and −6698 J/mol) imply spontaneity of the JGD adsorption onto AC. The overall data support that AC derived from locally low-cost (Iraqi chicken eggshells) may be suitable for the depollution of cationic dyes from water. Finally, several strategies have been proposed to scale up the current method for large-scale applications, including surface modification with metal oxide nanoparticles and chemical activation using various acidic and basic chemical agents.

Acknowledgments

The authors would like to thank the Chemistry department, College of Education for pure science Ibn Al-Haitham for facilitating this research work.

Disclosure statement

No potential conflict of interest was reported by the author(s).

ORCID

Dhafir T.A. Al-Heetimi http://orcid.org/0000-0003-3694-8234

References

[1] A. Mohagheghian, K. Ayagh, K. Godini and M. Shirzad-Siboni, Part Sci. Technol. **37** (3), 358 (2019). doi:10.1080/02726351.2017.1376363

[2] K. Mensah, H. Mahmoud, M. Fujii, M. Samy and H. Shokry, Biomass. Conv. Bioref. **14** (12), 12945 (2024). doi:10.1007/s13399-022-03304-4

[3] N. Amani, A. Mohagheghian and M. Shirzad-Siboni, J. Community Health Res. **10** (3), 1 (2024).

[4] K.S. Baidya and U. Kumar, S. Afr. J. Chem. Eng. **35** (33), (2021). doi:10.1016/j.sajce.2020.11.001

[5] A.H. Jawad, R.A. Rashid, M.A.M. Ishak and L.D. Wilson, Desalin Water Treat. **57** (52), 25194 (2016). doi:10.1080/19443994.2016.1144534

[6] S.A. Gawad, R. Ghazy, S. Mansour, H. Ahmed and A.R. Ghazy, J. Fluoresc. **35** (1), 3363–3376 (2024). doi:10.1007/s10895-024-03723-8

[7] S. Saha, S. Bhattacharjee and J. Chowdhury, J. Biomol. Struct. Dyn. **40** (12), 5328 (2022). doi:10.1080/07391102.2020.1870156

[8] A. Mohagheghian, S. Hooshmand Rad, K. Ayagh and M. Shirzad-Siboni, J. Mazandaran Univ. Med. Sci. **32**, 146 (2022).

[9] B.M. Babalola and L.D. Wilson, J. Compos. Sci. **8** (10), 414 (2024). doi:10.3390/jcs8100414

[10] S.M. Wabaidur, M.A. Khan, M.R. Siddiqui, M. Otero, B.H. Jeon, Z.A. Alothman and A.A. H. Hakami, J. Mol. liq. **317**, 113916 (2020). doi:10.1016/j.molliq.2020.113916

[11] Z.A. ALOthman, Materials **5** (12), 2874 (2012). doi:10.3390/ma5122874

[12] M.A. El-Kemary, I.M. El-Mehasseb, K.R. Shoueir, S.E. El-Shafey, O.I. El-Shafey, H.A. Aljohani and R.R. Fouad, J. Dispers. Sci. Technol. **39** (6), 911 (2018). doi:10.1080/01932691.2017.1410829

[13] O.A. Adelaja, A.C. Bankole, M.E. Oladipo and D.B. Lene, Int. J. Energ. Water Res. **3** (1), 1 (2019). doi:10.1007/s42108-019-00012-0

[14] K. Litefti, M.S. Freire, M. Stitou and J. González-Álvarez, Sci. Rep. **9** (1), 16530 (2019). doi:10.1038/s41598-019-53046-z

[15] S.L. Chan, Y.P. Tan, A.H. Abdullah and S.T. Ong, J. Taiwan Inst. Chem. Eng. **61**, 306 (2016). doi:10.1016/j.jtice.2016.01.010

[16] F. Amran and M.A. Zaini, Environ. Technol. Innov. **23**, 10172 (2021). doi:10.1016/j.eti.2021.101727

[17] V. Yönten, N.K. Sanyürek and M.R. Kivanç, Surfaces Interface. **20**, 100529 (2020). doi:10.1016/j.surfin.2020.100529

[18] L. Chen, T. Ji, L. Mu, Y. Shi, L. Brisbin, Z. Guo, M.A. Khan, D.P. Young and J. Zhu, RSC Adv. **6** (3), 2259 (2016). doi:10.1039/C5RA19616G

[19] C. Djilani, R. Zaghdoudi, F. Djazi, B. Bouchekima, A. Lallam, A. Modarressi and M. Rogalski, J. Taiwan Inst. Chem. Eng. **53**, 112 (2015). doi:10.1016/j.jtice.2015.02.025

[20] J. Wu, J. Yang, G. Huang, C. Xu and B. Lin, J. Clean. Prod. **251**, 119717 (2020). doi:10.1016/j.jclepro.2019.119717

[21] A. Mittal, M. Naushad, G. Sharma, Z.A. Alothman, S.M. Wabaidur and M. Alam, Desalin Water Treat. **57** (46), 2186 (2016). doi:10.1080/19443994.2015.1125805

[22] M.A. Khan, A.A. Alqadami, S.M. Wabaidur, M.R. Siddiqui, B.H. Jeon, S.A. Alshareef, Z. A. Alothman and A.E. Hamedelniel, J. Hazard. Mater. **400**, 123247 (2020). doi:10.1016/j.jhazmat.2020.123247

[23] A. Ahmad, D. Jini, M. Aravind, C. Parvathiraja, R. Ali, M.Z. Kiyani and A. Alothman, Arab. J. Chem. **13** (12), 8717 (2020). doi:10.1016/j.arabjc.2020.10.002

[24] M. Aravind and M. Amalanathan, Mater. Today Proc. **43**, 1491 (2021). doi:10.1016/j.matpr.2020.09.311

[25] M.A. Al-Kazragi and D.T. Al-Heetimi, Desalin Water Treat. **230**, 276 (2021). doi:10.5004/dwt.2021.27403

[26] D. Ramutshatsha-Makhwedzha, A. Mavhungu, M.L. Moropeng and R. Mbaya, Heliyon **8** (8), e09930 (2022). doi:10.1016/j.heliyon.2022.e09930

[27] E.R. Kenawy, A.A. Ghfar, S.M. Wabaidur, M.A. Khan, M.R. Siddiqui, Z.A. Alothman, A. A. Alqadami and M. Hamid, J. Environ. Manage. **219**, 285 (2018). doi:10.1016/j.jenvman.2018.04.121

[28] D. Dimbo, M. Abewaa, E. Adino, A. Mengistu, T. Takele, A. Oro and M. Rangaraju, Results Eng. **21**, 10191 (2024). doi:10.1016/j.rineng.2024.101910
[29] E. Moaveni, E. Keshmirizadeh and H. Modarress, Desalin Water Treat. **67**, 309 (2017). doi:10.5004/dwt.2017.20263
[30] J. Kochito, A. Gure, N. Abdissa, T.T. Beyene, O.E. Femi and A. Nayak, Sci. World J. **1**, 1–17 (2024). doi:10.1155/2024/7585145
[31] M.A. Al-Kazragi, D.T. Al-Heetimi and O.S. Al-Khazrajy, Desalin Water Treat. **145**, 369 (2019). doi:10.5004/dwt.2019.23609
[32] M. Tahergorabi, A. Esrafili, M. Kermani and M. Shirzad-Siboni, Desalin Water Treat. **57** (42), 19834 (2016). doi:10.1080/19443994.2015.1106351
[33] R. Askari, F. Mohammadi, A. Moharrami, S. Afshin, Y. Rashtbari, M. Vosoughi and A. Dargahi, Appl Water Sci. **13** (90), (2023). doi:10.1007/s13201-023-01899-1
[34] H. Ouaddari, B. Abbou, I. Lebkiri, A. Habsaoui, M. Ouzzine and R.F. Allah, Chem. Phys. impact. **8**, 100405 (2024). doi:10.1016/j.chphi.2023.100405
[35] S. Lagergren, Kongl. Vetensk. Acad. Handl. **24** (1), (1898).
[36] Y.S. Ho and G. Mckay, J. Environ. Sci. Heal A. **34** (5), 1179 (1999). doi:10.1080/10934529909376889
[37] M.A. Al-Kazragi and D.T. Al-Heetimi, J. Phys. Conf. Ser. **1879** (2), 02207 (2021). doi:10.1088/1742-6596/1879/2/022073
[38] I. Langmuir, J. Am. Chem. Soc. **40** (9), 1361 (1918). doi:10.1021/ja02242a004
[39] M.M. Haring, J. Chem. Educ. **3** (12), 1454 (1926). doi:10.1021/ed003p1454.2
[40] M.I. Tempkin and V.J.A.P.C. Pyzhev, Acta Phys. Chim. USSR. **12**, 327 (1940).
[41] Z. Medjdoubi, M. Hachemaoui, B. Boukoussa, A. Hakiki, A. Bengueddach and R. Hamacha, Mater. Res. Express. **6** (8), 085544 (2019). doi:10.1088/2053-1591/ab2732
[42] A. Dargahi, M.R. Samarghandi, A. Shabanloo, M.M. Mahmoudi and H.Z. Nasab, Biomass Conv. Bioref. **13** (9), 7859 (2023). doi:10.1007/s13399-021-01601-y
[43] L.A. Mohammed, A.S. Farhood and I.N.A. Ali, Eng. Technol. J. **32** (13), 3106 (2014). doi:10.30684/etj.32.13A.3
[44] K.Z. Elwakeel, A.M. Elgarahy and S.H. Mohammad, J. Environ. Chem. Eng. **5** (1), 578 (2017). doi:10.1016/j.jece.2016.12.032
[45] I.M. Radhi, S.S. Abd, R.A.S. Faraj, A.M. Abas and T.A. Himdan, Mong. J. Chem. **25** (52), 19 (2024). doi:10.5564/mjc.v25i52.3450
[46] N. Ayawei, A.N. Ebelegi and D. Wankasi, J. Chem. **2017**, 3039817 (2017). doi:10.1155/2017/3039817
[47] R. de Oliveira Zonato, B.R. Estevam, I.D. Perez, V.A. dos Santos Ribeiro and R.F. Boina, Clean Chem. Eng. **2**, 100023 (2022). doi:10.1016/j.clce.2022.100023
[48] A.H. Jawad, A.S. Abdulhameed, S.N. Surip and S. Sabar, J. Environ. Anal. Chem. **102** (18), 6189 (2022). doi:10.1080/03067319.2020.1807966
[49] H.K. Alzahrani, D.F. Katowah and H. Xiao, Int. J. Polym. Sci. **2024** (1), 1899137 (2024). doi:10.1155/2024/1899137
[50] M.A. Al-Kazragi, D.T. Al-Heetimi and L.D. Wilson, Int. J. phytoremediation. **26** (5), 639 (2024). doi:10.1080/15226514.2023.2259989
[51] S.H. Teo, C.H. Ng, A. Islam, G. Abdulkareem-Alsultan, C.G. Joseph, J. Janaun, Y.H. Taufiq-Yap, S. Khandaker, G.J. Islam, H. Znad and M.R. Awual, J. Clean. Prod. **332**, 130039 (2022). doi:10.1016/j.jclepro.2021.130039
[52] N. Jahan, H. Roy, A.H. Reaz, S. Arshi, E. Rahman, S.H. Firoz and M.S. Islam, Case Stud. Chem. Environ. Eng. **6**, 100239 (2022). doi:10.1016/j.cscee.2022.100239
[53] I. Ali, O.M. Alharbi, Z.A. Alothman, A.M. Al-Mohaimeed and A. Alwarthan, Environ. Res. **170**, 389 (2019). doi:10.1016/j.envres.2018.12.066
[54] A.K. Al-Jaafari, M.A.U.R. Al-Kazragi and A.K. Nayak, Sci. World J. **1** (1), 9799127 (2024). doi:10.1155/2024/9799127